Investigation on the compressive strength and durability properties of alkali-activated slag mortar: Effect of superabsorbent polymer dosage and water content

Developments in the Built Environment 17 (2024) 100322

Contents lists available at ScienceDirect

Developments in the Built Environment

journal homepage: www.sciencedirect.com/journal/developments-in-the-built-environment

Investigation on the compressive strength and durability properties of alkali-activated slag mortar: Effect of superabsorbent polymer dosage and water content

Peng Shi [a], Devid Falliano [a,*], Federico Vecchio [a], Giuseppe Carlo Marano [a]

[a] Department of Structural, Building and Geotechnical Engineering, Politecnico di Torino, Corso Duca Degli Abruzzi, 24, 10129 Turin, Italy

ARTICLE INFO

Keywords:
Internal curing
Superabsorbent polymer
Alkali-activated slag
Shrinkage
Durability

ABSTRACT

This paper presents the properties of alkali-activated slag (AAS) mortar additivated with a superabsorbent polymer (SAP) to improve its mechanical and durability properties. The effect of different dosages of SAP (0.0–0.3% with respect to the blast furnace slag weight) and different extra water additions on setting time, autogenous shrinkage, compressive strength, water permeability, frost resistance, heat of hydration, and porosity is presented and discussed. The results highlight the beneficial effect of adding SAP on the mechanical and durability properties of the proposed mixtures. Only at higher percentages of SAP and additional water occur performance drops due to excessive macro-porosity of the system. It is interesting to point out that, in contrast, shrinkage always decreases as the percentages of SAP addition and additional water increase, although it cannot be completely eliminated. Experimental evidence also highlights that significant benefits can be gained from using this material in harsh environments.

1. Introduction

In recent years, with the gradual deterioration of global ecological environment problems such as climate warming, acid rain spreading, and energy depletion, people's awareness of protecting the environment is also gradually increasing. Therefore, researchers have been exploring a green and environmentally friendly material that can replace ordinary Portland cement (OPC) in concrete structures (Chen et al., 2019). Industrial slag considered waste or by-product, can be fully utilized under the action of an alkali activator (Provis, 2014). The production of alkali-activated material is characterized by lower heat release than OPC (van Deventer JSJ et al., 2012). These wastes, which can be alkalized to stimulate their volcanic ash activity, are known as geopolymers. Moreover, energy consumption for production is reduced by more than 40 % compared with traditional cement, and the carbon dioxide emission is only 1/2–3/4 of cement (Mavroulidou and Shah, 2021; Turner and Collins, 2013; Ye and Radlińska, 2017). The contribution of each step to CO_2-e, from the purchase of raw materials to the production and construction of 1 cubic meter of concrete, is shown in Fig. 1. Turner et al. (Turner and Collins, 2013) believed that the alkali activator consumed a large amount of energy in the production process, with the geopolymer binder contributing 201 kg CO_2-e/m^3 and the OPC contributing 269 kg CO_2-e/m^3. Among them, the main components of slag (SiO_2, Al_2O_3, CaO, and Fe_2O_3 et al.) under alkaline conditions, it generates the ceramic body structure with silicon and aluminum as the main structural units. The material is mainly connected by ionic bonds and covalent bonds, and there are no coarse crystals such as ettringite or calcium hydroxide, which constitutes a three-dimensional network structure with high strength and stability. Therefore, alkali-activated slag (hereafter indicated as AAS) may have excellent mechanical properties and durability (Adediran et al., 2023; Pacheco-Torgal et al., 2012).

However, one of the main shortcomings of AAS is the significant shrinkage and the fast setting, owing to the characteristics of the material itself (Kalina et al., 2020). Moreover, the greater the amount of slag used in the precursor, the higher the autogenous shrinkage of the AAS slurry, which involves certain security risks to the structure (Huang et al., 2022; Ye et al., 2017). For example, cracking caused by shrinkage stress and other durability problems limit the practical application of AAS in engineering (Neto et al., 2008; Chen et al., 2023; Wang et al., 1995; Collins and Sanjayan, 2000). To solve this key technical problem, many scholars (Ye and Radlińska, 2017; Chen et al., 2023; Kumarappa et al., 2018; Song et al., 2016; Sakulich and Bentz, 2013; Zhao et al., 2019) have conducted relevant research on this topic. Philleo (1991) proposed the concept of internal curing as early as 1991. Tu et al.

* Corresponding author. Politecnico di Torino, Italy.
E-mail address: devid.falliano@polito.it (D. Falliano).

https://doi.org/10.1016/j.dibe.2024.100322
Received 8 November 2023; Received in revised form 24 December 2023; Accepted 3 January 2024
Available online 8 January 2024

(2018), Lee et al. (2018) and Cusson et al. (Cusson and Hoogeveen, 2008) reported investigations on different curing methods and conditions to verify their reliability. Lee et al. (2018), for example, reported that recycled aggregate as an internal curing agent could effectively reduce the autogenous shrinkage of the AAS system without affecting the strength. Oh and Choi (2018) showed that superabsorbent polymer (hereafter denoted as SAP) played a crucial role in reducing the shrinkage of AAS mortar. Ye and Radlińska (2017) indicated that high-temperature curing could optimize the aggregation or combination between adjacent calcium aluminosilicate hydrate (C-A-S-H) nanoparticles, improving the stability of C-A-S-H and reducing the shrinkage. Trincal et al. (2022) found that the introduction of metakaolin delayed the formation of AAS main hydration products such as aluminum-modified calcium silicate hydrate gel, and significantly reduced pore pressure, thereby diminishing the chemical shrinkage of pastes. Yuan et al. (2017) highlighted that if a small amount of limestone powder (≤30 vol%) is added, the autogenous shrinkage of the slurry increases, and once the addition amount is greater than 50 vol%, the autogenous shrinkage of AAS decreases, but the drying shrinkage increases with the raise of the content of limestone powder. The results of Ma et al. (2020) show that the addition of 3% shrinkage reducing admixture (SRA, alkyl polyether) can shorten the drying shrinkage of alkali-activated coal gangue-slag mortar by 47.5%. Yang et al.'s (Yang et al., 2021) experiment found that the MgO-based expansion agent could significantly decrease the autogenous shrinkage of AAS. Especially when combined with SAP, it could promote the consumption of MgO, and still improve the shrinkage reduction effect.

Internal curing materials, such as lightweight aggregate and SAP, can rapidly release water to supplement the internal moisture of concrete. Due to the low strength of lightweight aggregate, the strength of concrete is significantly reduced. Conversely, SAP as an internal curing agent is considered to be the most effective method, which can effectively reduce the autogenous shrinkage and drying shrinkage of concrete and improve its performance and service life. The utilization of SAP particles can act as a "small-scale localized reservoir" within the concrete matrix for internal curing, which is part of the research work of the RILEM Technical Committee (Mechtcherine et al., 2021). These advantages are achieved through its low crosslinking degree of three-dimensional network space structure and the benefits of a large number of hydrophilic groups on the molecular chain; to this must be added the low environmental impact and low price (Shen et al., 2016). For example, Tu et al. (2018) indicated that when the SAP content increased to 0.5 wt%, the chemical shrinkage and autogenous shrinkage of alkali-activated slag-fly ash pastes could be reduced by 45 % and 85 %, respectively. Furthermore, Yang and Almeida et al. (Yang et al., 2022a; Almeida and Klemm, 2018) also found that SAP, as an internal curing agent, can effectively compensate for the decrease in internal relative humidity of the system and reduce the autogenous shrinkage caused by self-drying, balance the humidity difference and diminish the cracking tendency of the slurry. Schröfl et al. (2012) discovered that the water release effect of SAP could alleviate the shrinkage cracking of concrete caused by early hydration and surface drying evaporation. Vafaei et al. (2019) considered that SAP has a strong liquid absorption ability in pore solution, and SAP can dramatically reduce the self-shrinkage of AAS slurry, but the formation of large pores will cause the decrease of compressive strength. Fu et al. (2020) used micro silica and kaolin clay modified SAP as a novel additive. They found that the negative effect of SAP additives on the compressive strength of AAS conglomerates could be reduced, as well as the tendency for the development of early drying shrinkage.

Several studies reported (Yang et al., 2022a; Zhang et al., 2022; Snoeck et al., 2015; Boshoff et al., 2020) the application of SAP in various conglomerates as internal curing agents and the optimization of specific properties, such as reducing self-shrinkage and drying shrinkage. However, since it is a synthetic polymer material, the differences in the water absorption capacity, type, dosage, particle size, or additional water diversion of SAP will cause differences in the test results (Tu et al., 2018; Schröfl et al., 2012; Mechtcherine et al., 2019; Tenório Filho et al., 2023). The application of SAP in the AAS system is still limited. In fact, for example, the water migration of SAP at different stages and the evolution of SAP's water absorption-release state, the changes of interface characteristics between SAP and paste after water release, the mechanism of SAP contraction in the AAS system and the mechanism of microstructure evolution need to be further investigated. Several studies have also been performed on the durability aspects of AAS, such as plastic shrinkage, permeability, and self-healing. It is well known that the shrinkage mechanism of AAS is more pronounced than that of OPC. In addition to reducing the modulus of the alkali activator and the alkali content, the incorporation of mineral additives, the addition of fibers, and the introduction of porous aggregates are also useful strategies for mitigating the shrinkage of alkali-activated slag composites, thanks to the densification of the paste microstructure, the increase in the formation of crystalline phases, and the reduction of the surface tension of the solution in the pores (Zhang et al., 2022). Although Bayati et al. (2023) found that self-healing of microcracks in the AAS matrix can be achieved through the microbial-induced calcium

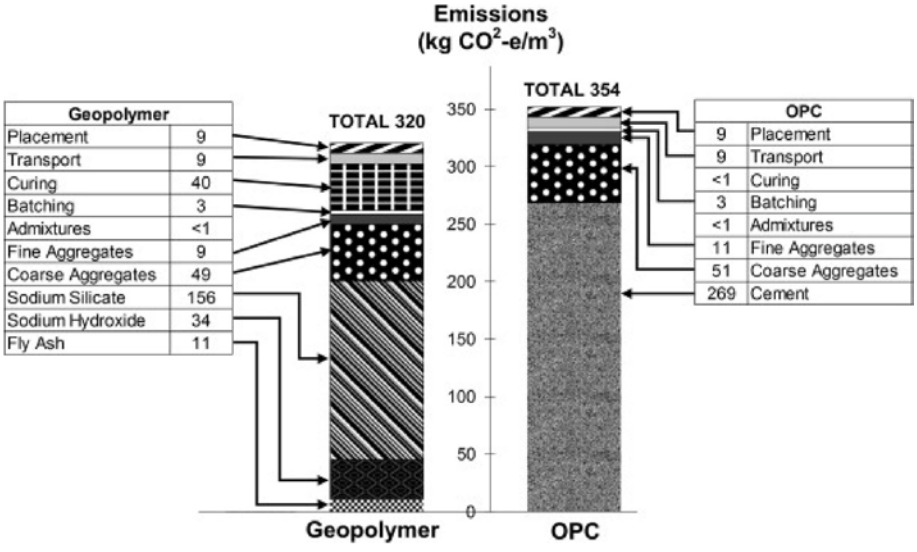

Fig. 1. Overviews of CO_2-emission with OPC and geopolymer systems (Turner and Collins, 2013).

carbonate precipitation technique, challenges persist in terms of bacterial cultivation conditions, viability concerns, and the need for increased technical expertise in specific survival environments. Nevertheless, SAP can also enhance the healing rate through the expansive effect within cracks and by promoting the formation of carbonate precipitation (Yang et al., 2023).

In fact, RILEM established a technical committee, 225-ASP, in 2007 to investigate the use of SAPs in concrete construction and the work was subsequently progressed by the new committee TC 260-RSC in 2014 (Mechtcherine et al., 2021; Boshoff et al., 2020). The report indicated that the presence of silica powder in the slurry increases the competitiveness of SAP in absorbing water from the surrounding matrix, thereby altering the rheological properties and workability of the fresh pastes. As reported, not all SAPs can effectively mitigate self-shrinkage, as SAPs, once rapidly desorbed, exhibits characteristics of ineffectiveness, preventing the attainment of the expected and desired internal curing effects (Mechtcherine et al., 2021). It is worth noting that the introduction of SAP as an admixture in cement-based materials contributes to enhancing freeze-thaw resistance (Mechtcherine et al., 2019). Furthermore, Tenório Filho et al. (Tenório Filho et al., 2023) found that reinforced concrete walls containing SAP maintained their original crack-free state even after two years and showed no signs of potential corrosion. Nevertheless, few studies have focused on the influence of SAP curing on the creep properties of cementitious materials and its application in AAS is currently limited to a preliminary stage and requires further development. Furthermore, due to the high water absorption and hydrating properties of SAP, investigations of SAP additions in AAS focused mainly on minimizing the drying shrinkage characteristics of the material. Therefore, beyond these fundamental aspects, this study presents an innovative approach by means of which SAP enhances the effectiveness of late-stage internal curing through pre-absorption, while maintaining an unsaturated state; this distinguishes the present study from both works in which dry particles are employed, and those in which fully saturated particles are used. Moreover, the effect on the different properties of AAS of the additional volume of water on the SAP was investigated. In particular, among other properties, this work highlights the effects of SAP on the AAS impermeability and frost resistance, providing an analysis of the mechanisms that led to the experimental evidence, and paving the way for their use in harsh climates. This study fits into this background and aims to explore whether the self-produced SAP with or without additional water diversion under pre-absorbent conditions affects the fluidity, compressive strength, autogenous shrinkage, frost resistance, and impermeability of AAS; the effects of different dosages of SAP are also presented and discussed. Hydration products, microstructure, and pore structure changes are characterized and described to clarify the influence of the amount of additional water and SAP content on the macroscopic properties of AAS mortar. Moreover, this study considers the fact that samples containing SAP diminish the real water-to-binder ratio by absorbing water from the capillaries of the slurry. To guarantee homogeneous dispersion of the SAP within the matrix and maximize the internal curing qualities, the SAP was preabsorbed without the use of an alkaline solution.

2. Materials and methods

2.1. Materials and mix design

The precursor was S95 grade blast-furnace slag (hereafter indicated as BFS or slag) which was purchased from Longze water purification company, Shanxi, China. The main chemical components of BFS are shown in Table 1. According to the ground granulated blast furnace slag used for cement and concrete, the basicity coefficient M_0 of the BFS is 1.58 (>1.0), the activity factor M_n is 0.59 (>0.25), and the mass coefficient K is 2.94 (≥1.2). These three parameters indicate that this BFS is a highly reactive and good quality alkaline slag. The density of BFS is 2.91 g/cm^3. The X-ray diffraction (XRD) pattern and scanning electron microscopy (SEM) image of BFS are shown in Fig. 2 (a) and Fig. 3 (a), respectively. The main components of slag are some amorphous phases and its surface is rough.

Table 1
Chemical compositions of BFS and water glass (wt.%).

Oxide composition	Blast-furnace slag (BFS)	Water glass
Calcium oxide (CaO): %	47.0	–
Silica (SiO_2): %	21.9	26.5
Alumina (Al_2O_3): %	13.0	–
Magnesium oxide (MgO): %	8.1	–
Sulfur trioxide (SO_3): %	2.5	–
Titanium dioxide (TiO_2): %	0.9	–
Ferric oxide (Fe_2O_3): %	0.7	–
Potassium oxide (K_2O): %	0.4	–
Manganese oxide (MnO): %	0.4	–
Sodium oxide (Na_2O): %	0.3	8.3
Hydrogen oxide (H_2O): %	–	65.2
Loss on ignition: %	2.3	–
Sum: %	97.5	100

The SAP selected for the test is a polyacrylic acid system, which mainly uses the sol-gel method of acrylic acid, methacrylic acid, acrylamide, hydroxypropyl acrylate, and other raw materials through hydrolysis and condensation reactions to form a three-dimensional network structure gel. After heat treatment and gelation, multi-polymer SAP powder particles, with a non-uniform particle size distribution, are obtained by processes such as drying and grinding (Fig. 2(b)). The bulk density and the moisture content of white powder polyacrylic acid SAP were 572 kg/m^3 and 3.5% respectively, which were insoluble in water. The SAP particles are irregular and broken polymer with a large size distribution, as shown by the particle size distribution (Fig. 2 (b)) and SEM image (Fig. 3 (b)). Interestingly, the hydrophilic groups ionize when water is absorbed, allowing the ionized cations to flow freely throughout the solution, while the anions on the high-polymer molecular chains of SAP remain intact (Yang et al., 2022b), as illustrated in Fig. 4.

The alkaline silicate solution is a mixture with a modulus of 0.93, obtained by adding sodium hydroxide to adjust the initial modulus of water glass. The mass ratio of sodium hydroxide, water glass, and tap water is 1: 3.64: 4.55. Sodium hydroxide (purity ≥96 wt%) is a white flake provided by Shanghai Pharmaceutical Group. Water glass with 8.3 wt% Na_2O and 26.5 wt% SiO_2 is a viscous transparent liquid with an initial modulus of 3.3, and the solid content is 34 %. The alkaline solution needs to be prepared at least 8 h before the test to ensure uniform heat dissipation and return to indoor temperature.

The fine aggregate used is standard sand with density of 2630 kg/m^3; particle size and mud content are lower than 5 mm and 0.20%, respectively. The particle size distribution of the sand meets the standard requirements and belongs to zone II medium sand.

In previous studies (Kalina et al., 2020; Song et al., 2016; Tu et al., 2018; Zhang et al., 2022), SAP dry powder was added directly; however, this cannot ensure that the SAP absorbed the free water adequately to achieve the desired internal curing effect. Furthermore, the addition of dry powder also resulted in the loss of mixing water in the fresh state of pastes due to absorption and in sticking together SAP particles, thus reducing the workability, and improving the chance of drying shrinkage of the matrix. In fact, most of the mixed water is absorbed by cementitious materials and sand, and the characteristics of internal curing materials cannot be fully exerted. Conversely, complete water saturation may lead to premature release of stored water of SAP after its addition to slurry owing to osmotic and capillary pressures as well as ion concentration differences (Yang et al., 2022b), affecting the long-term curing effect. Pre-wetted SAP not only has less impact on the compatibility of fresh mortar but also improves the early-dimensional stability of the concrete structure. The gel-like state of presoaked SAPs can reduce clumping and improve the integration of SAPs with the surrounding

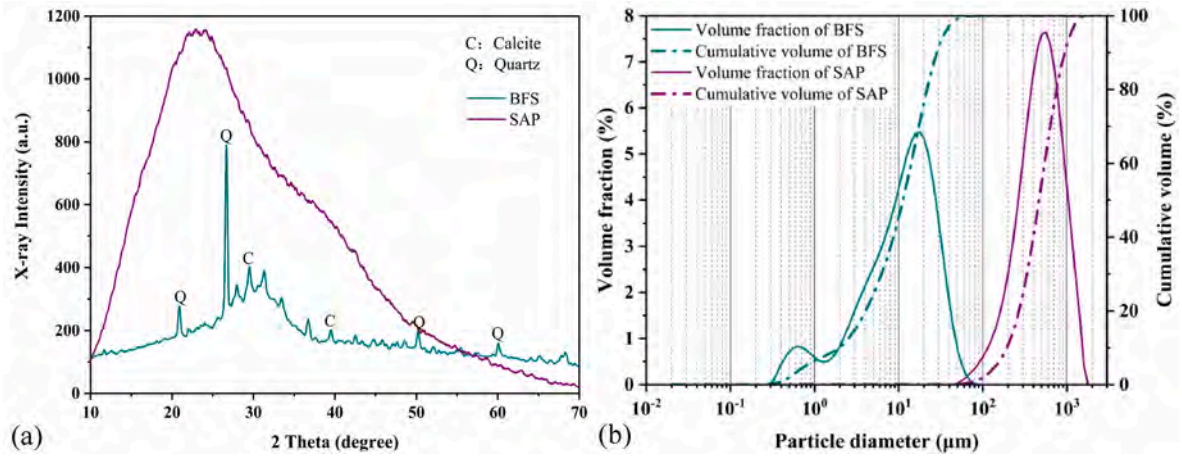

Fig. 2. XRD pattern of the BFS and SAP (a); Particle size distribution of BFS and SAP (b).

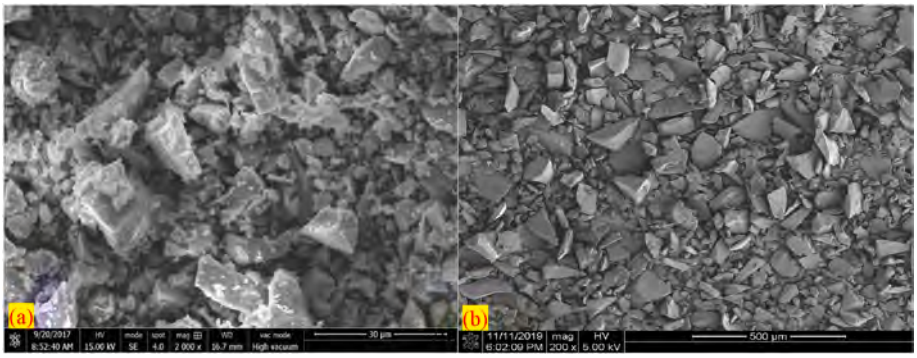

Fig. 3. SEM image of BFS (a) and dry SAP particles (b).

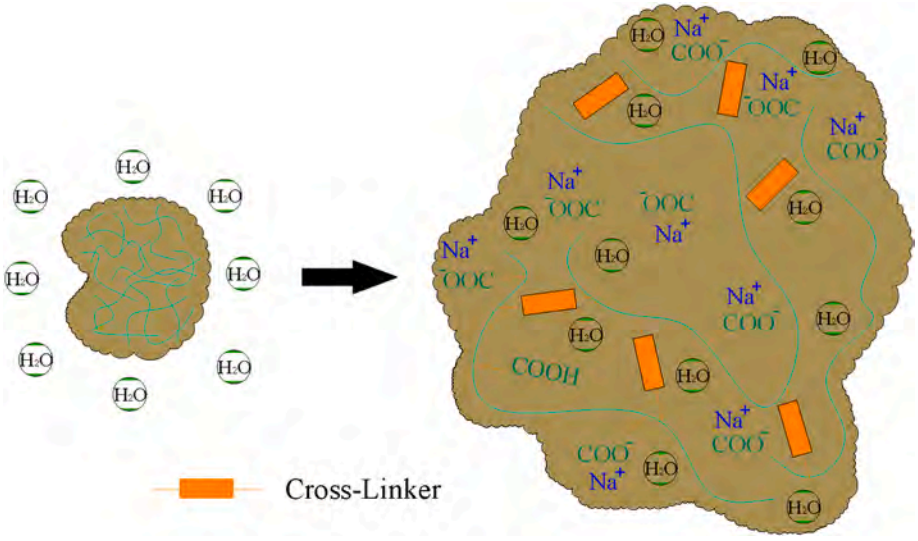

Fig. 4. Diagram of the changes in the internal anionic and cationic structure of SAP before and after water absorption (Yang et al., 2022b).

medium. Hence, the SAP powders, which had pre-absorbed water for 5 min, were mixed with the dry raw material for 1 min, and then slowly poured into the alkaline solution and stirred for another 3 min before sealing them into the mold for curing.

Table 2 shows the mix proportions of the mixtures presented in this study. In this table, the column extra water-to-binder ratio reports any possible further additions of water in the mixtures of the studied SAP-AAS mortars. In fact, due to the absorption of a part of the alkali solution in the early stage of pre-saturated SAP, the actual water-to-binder ratio is reduced. To ensure that workability is not adversely affected, based on the Power model (Powers and Brownyard, 2003), and according to the performance index of SAP itself and previous related studies, additional water was introduced at the ratios m_{SAP}:m_{water} = 1:15 and 1:25; therefore, the effect of different extra water on the

Table 2
Mix proportions of SAP-AAS mortar.

Code	BFS[a] (wt %)	SAP (wt %)	Water glass (Na_2SiO_3, wt. %)	Binder-sand ratio	Alkaline activator ratio (Na_2SiO_3/NaOH)	Extra water-binder ratio	Total water-binder ratio
S0		0				0	0.360
S0.1W0		0.1				0	0.360
S0.2W0		0.2				0	0.360
S0.3W0		0.3				0	0.360
S0.1W15	100	0.1	20.39	0.56	3.67	0.013	0.373
S0.2W15		0.2				0.027	0.387
S0.2W25		0.2				0.045	0.405
S0.3W15		0.3				0.040	0.400

[a] Blast-furnace slag was cumulated to 100%, and the other materials were added in corresponding proportion.

properties of the proposed AAS mixes was further explored. In some previous studies (Yang et al., 2022b, 2022c), 0.2 wt% was considered the optimal dose of SAP to exhibit excellent performance in the wet mixing state. Additionally, the typical doses of 0.1 wt% and 0.3 wt% of SAP were added in this study and thus they were argued as well for mitigating shrinkage. In all the AAS mortars, the base water-to-binder ratio was 0.36, while the alkali content was calculated as Na_2O equivalent. The alkaline activator was added to 4% Na_2O-equivalent, and the SAP content was 0.1%, 0.2%, and 0.3% of the BFS mass.

2.2. Absorption

The peculiarity of SAP to be characterized by good water absorption capacity is the premise of internal curing materials. Tea-bag method (Tu et al., 2018; Yang et al., 2022a) was used to test the changing trend of water absorption capacity of sodium polyacrylate SAP with time at different value of pH; pH = 7 (deionized water), pH = 7.6 (tap water), and pH = 12.8 (the supernatant of AAS paste), respectively. This evaluation is closer to the actual working condition than evaluations performed in previous studies (Tu et al., 2018), in which absorption capacity was determined directly with the alkaline solution. Nevertheless, the existence of charge compensation, calcium ions and aluminum ions in the actual environment will affect the water absorption capacity of SAP (Tenório Filho et al., 2023). According to Table 2, 10 g of reference group samples, after one day of curing, were taken and ground into powder. Then, 500 mL of deionized water was added to the oscillator for vibration for 1 day; the supernatant of AAS paste was obtained via filtration. A gram of dry SAP powder was put into the bottom of a pre-wet nylon bag that had a maximum pore size of 0.074 mm, allowing the materials to pass through, and the bag was then placed in a beaker holding 500 mL of a pH-known solution. This operation was repeated for three different pHs. The sealing film was used to seal the cup-mouth so that it could absorb water statically. First, the evaluation is carried out every 2 min; after 10 min, the evaluation is carried out every 5 min; and finally, after 30 min, the evaluation is carried out every 10 min until roughly identical evaluations are obtained.

As illustrated in Fig. 5, regardless of the pH of the solution SAP showed strong water absorption ability in the first 8 min, and then began to decline until the curve was flat. Moreover, as the pH changes, the time when the curve reaches the highest point is also different. The SAP has the strongest absorption capacity at pH = 7, at which it can reach 233.9 times its own weight, followed by pH = 7.6; in the case of pH = 12.8, the absorption rate is about 13% of that obtained for pH = 7. This is because the external ions (e.g., Al^{3+} and Ca^{2+}) further change the intermolecular and intramolecular interaction forces of SAP via the electronic barrier effect of molecular chains (Boshoff et al., 2020). In addition, there is osmotic pressure between the internal and external portion of SAP due to the difference of ion concentration, and this osmotic pressure decreases with the increase of ion concentration in the solution, which weakens the water absorption ability of SAP (Schröfl et al., 2012).

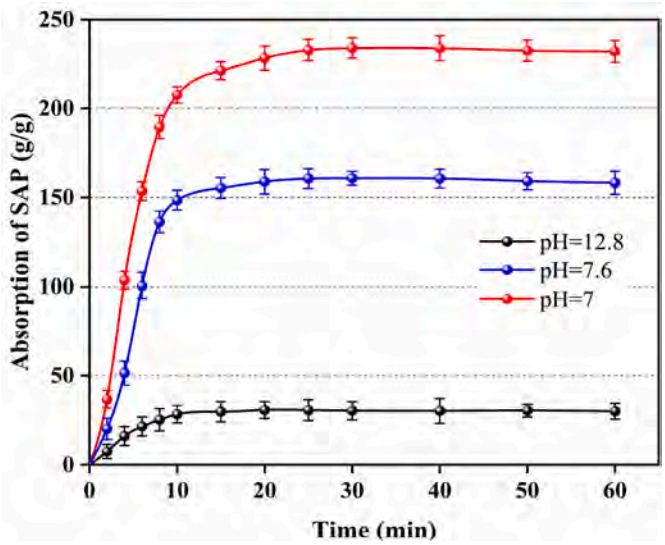

Fig. 5. Absorption of SAP in three different pH solutions with tea-bag method.

2.3. Mechanical behavior

The initial and final setting times of the samples were measured by a Vicat apparatus (Boshoff et al., 2020). The compressive strength of the AAS mortar was tested on prismatic specimens of dimensions 4 cm × 4 cm × 16 cm using YAW-300C automatic testing machine according to ASTM C349-18 (ASTM, 2018). The compression testing frame was used to ensure the compression area of 4 cm × 4 cm. The load was applied at a rate of 1.5 MPa/s. The curing ages of specimens were 3, 7, 28, and 56 days, respectively. The specimens were cured in a climatic chamber with 98% humidity at 20 ± 2 °C. Three samples from each age were measured and averaged.

2.4. Autogenous shrinkage

Shrinkage is a key factor in characterizing the volumetric stability and long-term durability of concrete and therefore guaranteeing low shrinkage is necessary. Furthermore, the high shrinkage of AAS increases the risk of cracking, especially with water glass as an alkaline activator. Internal curing is thought to reasonably weaken the self-shrinkage produced by AAS mortar systems due to the volume change of pastes before and after the chemical reaction, and SAP is also considered to be the most potential and widely used internal curing agent (Sakulich and Bentz, 2013; Tu et al., 2018; Yang et al., 2023; Powers and Brownyard, 2003). The autogenous shrinkage of AAS paste was measured by NS–NC–12 channel cement mortar shrinkage tester with bellows length of 425 mm and outer diameter of 29 mm referring to ASTM C1698-19 (ASTM, 2014). Before testing, calibration of the micrometers and corresponding channels of the measuring instrument was

carried out. During the test, the fresh slurry was layered and slowly poured into the mold, and then put into the shaking table for compaction to reduce air entrained. Temperature and relative humidity were maintained at 22 °C and 65%, respectively. Autogenous shrinkage test took two bellows per group for testing.

2.5. Water permeability

To evaluate the impermeability of AAS mortar, truncated conical specimens were prepared, characterized by top diameter equal to 70 mm, bottom diameter equal to 80 mm, and height of 30 mm. The six samples per group were cured for 28 days at a temperature of 20 ± 2 °C and relative humidity greater than 95%. The inside of the test mold was wiped with a cloth without oil before molding. After the curing period, the sample side perimeter was sealed with sealing materials, and the six specimens were placed in the SS-15 mortar penetrator for the water permeability test referring to Chinese standard JGJ/T 70–2009 (JGJ/T, 2009). The samples were pressurized starting at 0.2 MPa; then, once a stable condition was reached, the pressure was gradually increased at 0.1 MPa until half of the six specimens in each mixture showed infiltration phenomena. Finally, the average maximum pressure was recorded and calculated according to the standard formula Eq. (1).

$$P = H - 1 \tag{1}$$

Where H is the highest water pressure on AAS mortar when osmotic occurs, MPa; P is the seepage pressure on AAS mortar, MPa.

2.6. Frost resistance

According to Chinese standard GB/T 50082-2009 (GB/T, 2009), cubic specimens with a size of 70.7 mm after 26 days of curing were taken out from the curing room and immersed in water at 15 °C ~ 20 °C for 2 days. The test group was treated with TR-CLD freeze-thaw cycle test machine (Nashi, Shanghai Tongrui), and the reference group was returned to the climatic room until the freeze-thaw cycle stopped. Then the experimental group and the reference group were subjected to compression tests. Regardless of the group, three mixture samples from each group were involved in the freeze-thaw cycle. Specifically, the samples were subjected to 200 (number of cycles) freeze-thaw cycles, with controlled temperature between −18 ± 2 °C and 16 ± 2 °C. Samples subjected to the freeze/thaw cycles were examined every 15 cycles, and the test was stopped if two of the three cubes that constituted each series were found to be severely damaged.

2.7. Heat flow

According to the mixture proportions without sand reported in Table 2, the hydration reaction rate and the total heat of AAS paste were tested by 8-channel isothermal calorimeter TAM Air for 7 days. The test temperature was kept at 21 ± 1 °C. The SAP was first weighed and placed in an ampoule within the same proportion of mixing water and stirred with a magnetic stirrer for 5 min. Approximately a total of 20 g of slurry (containing 10 g of slag) was placed in the bottom of the ampoules and then quickly homogenized and mixed. Next, the uniform mixtures were placed in the apparatus one after the other to collect the heat flow data.

2.8. Hydration products

From the core of the 28-day aged specimens, after breakage, an amount of about 5 g of material was taken and soaked in ethanol to stop hydration for at least 3 days. Then the samples were dried in a 60 °C vacuum drying oven to constant weight. The samples were ground into powder in an agate bowl containing 5 g anhydrous ethanol. About 50 mg of the sample powders were tested by Netzsch STA 449 C synchronous thermal analyzer (Germany). The test environment is helium. The temperature range was controlled at 25–1000 °C and the heating rate was kept at 10 °C/min.

Pieces of 5 mm were extracted from the core of the 28-day aged samples after their breakage; hydration was stopped by soaking them in ethanol solution for 3 days. After vacuum drying, the pieces were ground into powder until the maximum particle size was approximately 10 μm. The hydration products of AAS paste were analyzed by X'pert3 powder X-ray diffractometer (Panalytical, Netherlands) with an incident beam of Cu-Kα radiation for a 2θ scanning range of 10°–70° at 40 kV and 40 mA. The scan speed and step size of each sample were 5°/min and 0.02°, respectively.

2.9. Microstructure

Small samples of about 2–5 mm in length were taken from the 28-day cured AAS mortar samples. These samples were soaked in ethanol to stop hydration and then dried in vacuum drying oven. The microstructure of hydration products around SAP was observed by FEI Quanta 250 scanning electron microscope (resolution up to 0.8 nm) after the samples were metallized with gold.

The pore size analysis of the sample was tested by PoreMaster-60 automatic mercury intrusion porosimeter (MIP) of Quantachrome, USA. The minimum pore size measurement can reach 3 nm. After the samples were broken, small pieces with a particle size of about 5 mm were selected. Then the samples were immersed in anhydrous ethanol to stop hydration. The general specimen needs to be soaked for more than 48 h. Then, before the MIP test, the samples were vacuum dried at a temperature of 60 °C until constant weight was reached.

3. Results and discussion

3.1. Hardening and strength

Table 3 reports the initial and final setting time of each sample of AAS mortar. An expected phenomenon is the delay of the setting time as the SAP content increases; in any case, both the initial setting time and the final setting time generally remain higher than in the S0 case. This result can be explained by the lower initial porosity of the matrix because of the relevant adsorption properties of SAP. Because of this, structuration and flocculation phenomena inside the cementitious matrix occur faster, increasing the stiffness of the mixture. Alternatively, the introduction of extra water increases the actual water-to-binder ratio inside the mix and gives rise to an increase in the final setting time. Moreover, in this case, the expansion of SAP delays the early chemical reaction and increases the initial porosity ratio, resulting in a longer initial setting and final setting time (Snoeck et al., 2015). This experimental finding is consistent with the experimental results of Yang et al. (2022a).

The compressive strength of the AAS mortar is shown in Fig. 6. In summary, the compressive strength of AAS mortar samples increases first and then decreases with the increase of SAP dosage, regardless of with or without extra water. Specifically, the compressive strength of 0.2% SAP doses cured 28-day enhanced by 22.39% without additional

Table 3
Initial and final setting time of AAS specimens.

Specimens	Initial setting time (min)	Final setting time (min)
S0	9	23
S0.1W0	10	32
S0.1W15	18	41
S0.2W0	12	35
S0.2W15	22	47
S0.2W25	28	56
S0.3W0	20	48
S0.3W15	29	58

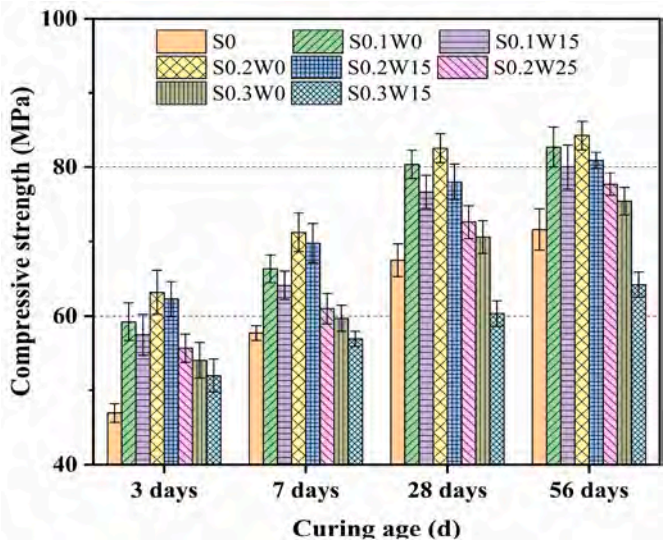

Fig. 6. Compressive strength of AAS mortars at various curing age.

water compared with the control group. Although the introduction of SAP dosage contributed to the development of strength, the excess introducing additional water reduced the strength by increasing the water voids due to the increase in the water-cement ratio. Obviously, too much SAP was similarly detrimental to the development of compressive strength. The compressive strength of S0.2W0 was the highest, which could reach 84.25 MPa at 56 days. Therefore, the optimal concentration of SAP is 0.2% by weight with respect to BFS. In any case, the compressive strength of other experimental groups was higher than that of S0 except for S0.3W15. As can be seen from the results, not only excessive SAP dosage, but also excessive additional water content led to lower compressive strength of AAS mortar. Instead, an adequate amount of SAP leads to increases in compressive strength as it can improve the degree of hydration of slag, intensify the internal hydration process, and increase hydration products, as will be highlighted in Section 3.6, 3.7 and 3.10. The reason for this is that the irregular pore shapes left by the release of water from SAP particles can create high stress concentrations and affect mechanical behavior. Furthermore, the introduction of 0.2% SAP facilitates strength development partly due to the increased degree of hydration of the AAS, and substantially reduces the self-shrinkage within the AAS matrix. Porosity reduction also leads to the improvements found, in fact, as will be shown, some hydration products are attached to the edge of the pores making the cementitious matrix denser.

Nonetheless, when SAP is used as an additive in cement-based materials, there could be some voids in the matrix (as will be shown later in Fig. 12), which could hurt the strength of the material (Yang et al., 2022a; Almeida and Klemm, 2018; Esteves et al., 2007). The air pores left by SAP shrinkage are also weak points in the materials structure (Mechtcherine et al., 2014). Therefore, even if shrinkage decreases, an excessive dosage of SAP may not be beneficial for mechanical strength. Regarding the influence of curing time, the compressive strength of all mixtures increased as the age of the samples increased, although the rate of increase in compressive strength diminished. It indicates that with the development of the hydration process, the concentration of OH^- in mortar gradually increases. When C(OH−) exceeds a certain threshold, the activity of slag is excited and reacts with sodium silicate rapidly. The generated hydration products will be attached to the surface of the slag to form a protective shell, which prevents the further hydration reaction and slows down the growth rate of compressive strength of mortar in the later stage (Chen et al., 2019). When extra water is introduced, the water absorption of SAP will be weakened in an alkaline, multi-ion, and high concentration environment, which is not enough to absorb all too much water. Thus, residual water would increase the porosity and the hardening time of the matrix (see Table 3), which is not conducive to the development of compressive strength of AAS mortar.

3.2. Linear autogenous shrinkage

Fig. 7 presents the effect of SAP dosage and additional water content on self-shrinkage curves of AAS paste at different times. The phenomenon of autogenous shrinkage is a characteristic of this type of material; such shrinkage is emphasized by the increase in surface tension due to the hydration reaction (Jensen and Hansen, 2001). With the increase of SAP content, the autogenous shrinkage value of AAS pastes decreased significantly. The contraction value of S0 in the control group increased rapidly after final setting time, reaching about 3990.59 μm/m on the 1st day and 7476.34 μm/m on the 35th day, while that of S0.3W0 was only 1480.32 μm/m on the 1st day and 2707.82 μm/m on the 35th day. SAP as an internal curing agent can balance the internal relative humidity of the system through the water absorption-release mechanism; this mechanism compensates for moisture and thus reduces the moisture difference between different portions of the element caused by water loss. All this leads to the reduction of concrete shrinkage and a consequent improvement in concrete durability (Sun et al., 2020; Zhong et al., 2019). When additional water was introduced, the decrease in the autogenous shrinkage value of AAS paste becomes more significant, and the autogenous shrinkage value of S0.2W25 at 35 days was reduced by 30.95 % compared with that of S0.2W0. Notwithstanding, if too much free water was introduced, the compressive strength would be greatly reduced (Fig. 6). However, regardless of the amount of SAP and additional water, shrinkage cannot be completely removed, which is also consistent with the research results of Snoeck et al. (Yang et al., 2021; Snoeck et al., 2015). With the amount of SAP and water increases, the reduction in shrinkage is accompanied by an increase in the compressive strength and impermeability of the AAS mortar (see Figs. 6 and 10).

In the early stage, SAP did not play an internal curing role due to the high internal humidity of the mixture. With the intense hydration reaction, the relative volume between the generated hydration products and the original reactants decreases, and the internal water is consumed to produce chemical shrinkage. As is well known, the hydration reaction releases heat: these temperature changes cause part of the water loss. Under the action of humidity difference, the internal moisture begins to migrate from high humidity area to low humidity area, resulting in autogenous shrinkage and drying shrinkage, which further aggravates the early shrinkage. The internal moisture therefore decreases and the

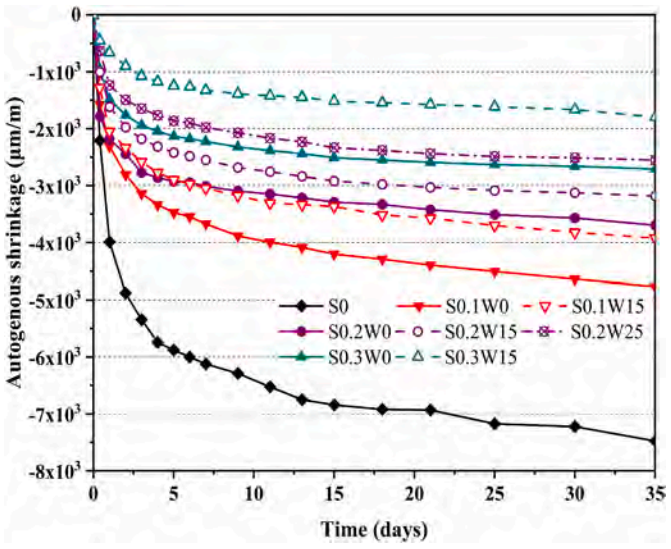

Fig. 7. Autogenous shrinkage of AAS pastes at various SAP dosage and extra water content.

SAP begins to release water under the negative pressure of the capillary pores, humidifying the dry capillary pores of the AAS paste, reducing capillary stress and, consequently, autogenous shrinkage of the pastes (Liu et al., 2017). Furthermore, increasing the dosage of SAP may give rise to a positive effect of internal curing on a larger volume of the sample, resulting in enhancement of the beneficial effect of shrinkage reduction previously explained. In addition, the presence of SAP can lead to better crack sealing capacity in concrete elements, where cracks could occur as a consequence of loads or environmental actions. As shown in (Snoeck et al., 2016), in fact, the high relative humidity and the incorporation of SAP contribute positively to the healing ability. By increasing the SAP dissolving rate and particle size, the efficacy of healing can be improved, as healing products consist mainly of calcium carbonate and less of calcium hydroxide (Lee et al., 2010).

3.3. Frost resistance

For some cold regions, it is extremely important that AAS mortars have good frost resistance. Fig. 8 depicts the surface morphological features of AAS mortar at 200 freezing and thawing cycles. Fig. 9 shows the effect of SAP dosage and additional water diversion on strength loss rate and mass loss rate of AAS mortar under different freeze-thaw cycles. With the increase of freeze-thaw cycles, the strength loss rate and mass loss rate of AAS mortar increase in turn, but as the dosage of SAP increases, the frost resistance of the mortar gradually improves. It is clear and easy to observe that as the number of freezes and thaws increases, the AAS mortar cracks and the surface paste begins to flake off, exposing the fresh matrix inside. The freeze damage seems to have less influence on the AAS mortar containing SAP, as shown in Fig. 8. However, the introduction of additional water can lead to increased surface damage due to increased capillary pressure and freezing expansion forces. In fact, the strength and mass-loss rates of S0.3W0 were reduced by 66.00% and 59.67%, respectively, compared with the reference group. The presence of SAP, as mentioned above, improves hydration, with the additional effect of reducing the spacing factor, which is correlated with improved frost resistance of the material (Filho et al., 2021). Besides, SAP, as an excellent "small-scale reservoir" of water migration, expands after absorbing water to form a gel, which can effectively alleviate the hydrostatic pressure and osmotic pressure caused by freeze-thaw changes. Due to freeze-thaw cycles, during freezing, the hydrostatic pressure of the unfrozen water that is generated can result in damage to the concrete; in this case, the SAP can absorb a large amount of water to form a gel, consequently reducing the pressure on the matrix. In addition, the formation of this gel could block, during the thawing phase, the entry of water to any cracks that have already occurred, improving the material's resistance to subsequent frost cycles. Lastly, after releasing water, SAP leaves a closed hole (as shown further below in Fig. 13), which provides a certain space for volume expansion, leading to the improvement of the frost resistance of AAS mortar (Ma et al., 2020; Winnefeld et al., 2020). However, the more extra water is introduced, the worse the frost resistance effect of AAS mortar, and as freeze-thaw cycles increase, the greater the reduction in strength and mass. Excessive introduction of internal curing water will increase the actual water-to-binder ratio and the amount of frozen water, which will enhance the average pore size of the internal void of the pastes. The frost resistance of concrete will be significantly reduced by the increase of micropores and macropores containing frozen water.

3.4. Water impermeability

The water impermeability results of the AAS mortar are shown in Fig. 10. It can be seen that S0.2W0 has the best water impermeability, increased by 60% compared to S0. In addition, the impermeability of AAS mortar decreases with the increase of additional water. Since SAP, as a superabsorbent material, has a strong water absorption and moisture retention capacity, it modifies the pore structure distributions of the matrix to make it more impermeable (Yang et al., 2022c). Because of the properties of SAP, there is an expansion of its volume due to water absorption during the early stages of hydration. This results in a lower amount of available free water and, in other words, a reduced effective water-to-binder ratio. Then, the SAP begins to gradually decrease in volume with the release of water during the drying process of the material, resulting in spherical holes in the AAS matrix. When the SAP content is less than the optimum, the inner pores are filled by the expanded SAP, this hinders water penetration into the specimen, improving the impermeability of the AAS mortar. However, once the dosages of SAP and extra water are too large (e.g., S0.3W15), the number of macropores introduced increases correspondingly. As already discussed and shown in Fig. 5, the associated compressive strength of the specimens decreases. This increase in matrix porosity also causes the presence of many interconnected pores in the specimen. Therefore, when water enters the specimen under pressure, these pores accelerate the passage of free water to some extent, which drops the impermeability of AAS mortar. So, the optimal dosage of SAP (0.2% with respect to BFS weight) and additional water diversion need to be considered for the impermeability of AAS mortar.

3.5. Hydration heat

Fig. 11 shows the effect of SAP dosage and additional water on the heat flow and accumulative heat of AAS pastes. The curves of heat flow of all mixtures exhibit two peaks. The first peak is generally produced by the wetting and the dissolution of the precursors (Sakulich and Bentz, 2013). Then after about 2~3 h of dormancy there is the second main peak, that is predominantly due to the formation of other phases, such as the aluminosilicate gel (Fang et al., 2018). It can be seen from Fig. 11(a) that the second peak heat flux generated by S0 is the largest, which is about 5.99 mW/g. When the SAP content without additional water increases from 0.1% to 0.3%, the peak heat flux also decreases from 5.63 mW/g to 5.14 mW/g. It indicates that the incorporation of SAP hinders the early chemical reaction of AAS pastes. In addition, the curve reaction peak gradually shifted to the right, indicating that the absorption characteristics of SAP may lead to the deceleration of the initial alkali reaction (Tu et al., 2018). This is consistent with the results of Yang et al. (2022a). Moreover, the gradual release of the activator from SAP can dilute the concentrations of Ca^{2+} and Al^{3+} in the original pore solution,

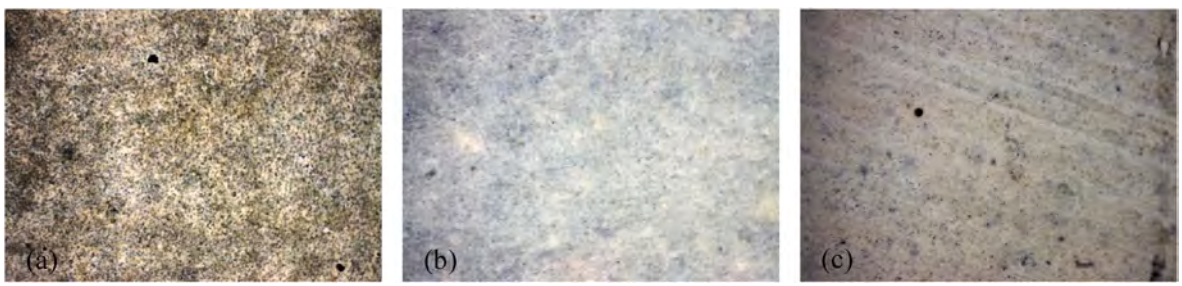

Fig. 8. Surface condition of AAS mortar under 200 freeze-thaw cycles at a 50× magnification. (a) S0, (b) S0.2W0, (c) S0.2W15.

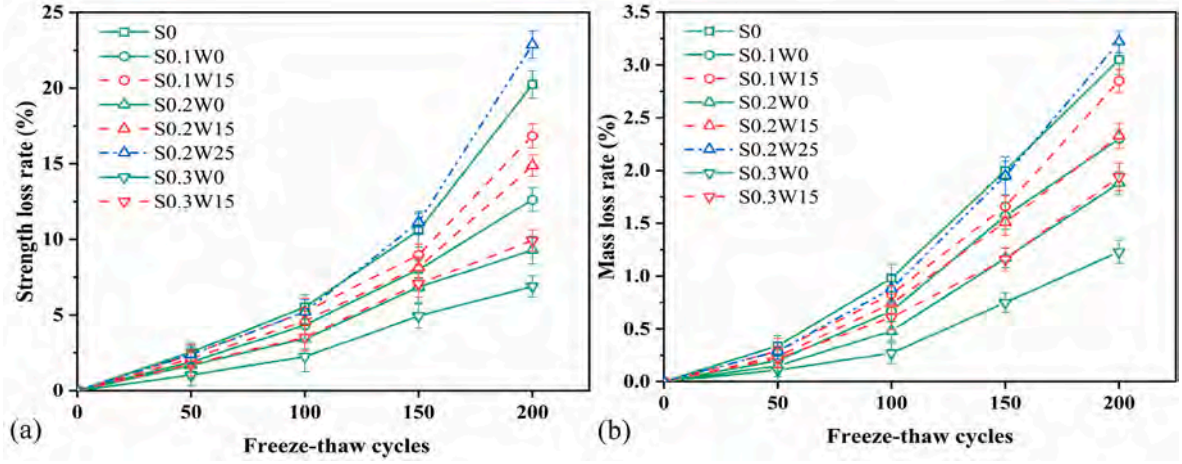

Fig. 9. Strength loss rate (a) and mass loss rate (b) of AAS mortar under different freeze-thaw cycles.

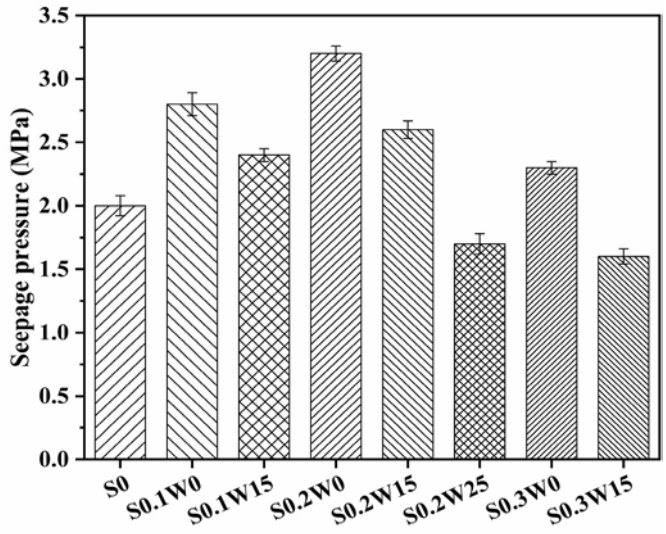

Fig. 10. Water impermeability of AAS mortar at various SAP dosage and additional water content.

thereby delaying the time when these ions reach the critical concentration (Almeida and Klemm, 2018). Nevertheless, the stored liquid in SAP will finally release and incorporate into the reaction, so as to improve the further degree hydration of the paste over the long-term. This view is congruent with the increased compressive strength of AAS mortar containing SAP, as shown in Fig. 6.

Once extra water is introduced, the corresponding peak decreases significantly. The addition of water dilutes the alkaline activator, reducing the peak hydration rate of slag. These initial hydration products may precipitate on the surface of slag to form a protective layer, which may prevent further hydration of slag. Mo et al. (2017) reported that excluding water, in the first few hours after SAP mixing, some alkali ions may also be absorbed by SAP, reducing the concentration of alkali solution and delaying the main peak. This also justifies the setting time results of each AAS pastes sample in section 3.1. As is shown in Fig. 11 (b), the SAP-incorporated mixtures accumulated more heat, i.e., a higher reaction degree, than the control group S0. As the water-to-binder ratio increases, the cumulative heat increases in turn; in particular, for S0.2W25, the cumulative heat still has an increasing trend even after 168 h of testing.

3.6. Thermal analysis

The incorporation of SAP facilitates strength development because it is more favorable for hydration products formation and pore structure distribution. Therefore, in order to better analyze the effect of SAP as well as additional water on the hydration products of AAS mortar, the amount of phase generation was characterized directionally by TG-DTG curves. Meanwhile, TG and XRD results can complement each other.

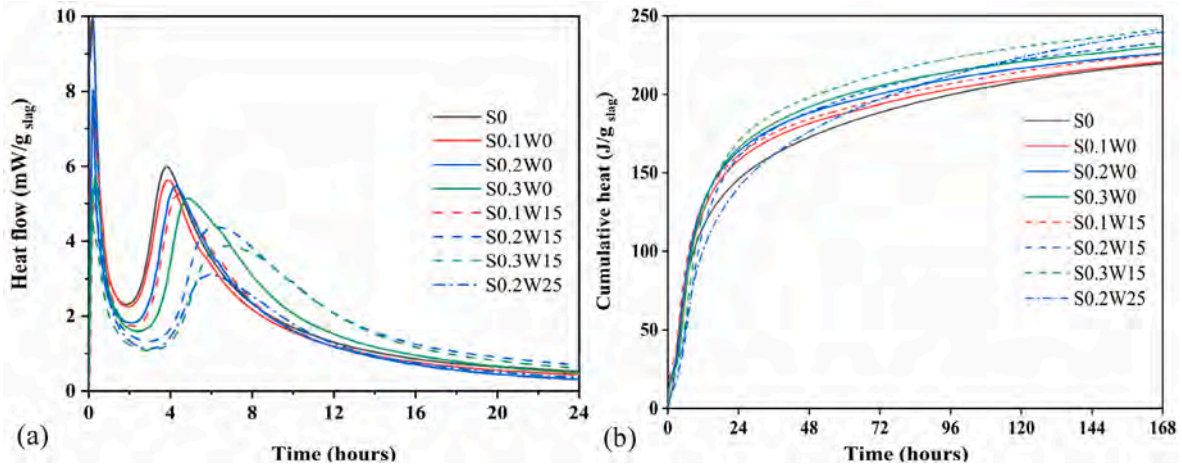

Fig. 11. Heat flow (a) and cumulative heat (b) of AAS pastes as a function of time.

Fig. 12 shows the TG/DTG curves of AAS pastes at different SAP dosage and additional water content at 28 days. The TG-DTG curves of all mixtures reveal the same characteristic trend, as shown in Fig. 12(a) and (b). The first peak occurs at a temperature generally lower than 250 °C and is mainly due to the evaporation of physical and chemical bonding water in the C-A-S-H and N-A-S-H gel structures (less 110 °C) and the loss of weak bonding water adsorbed by hydration products such as the ettringite (100–150 °C), hemicarbonate (150–180 °C), and AFm phases (180–200 °C) (Duxson et al., 2007). Overall, the mass loss occurs at 100–200 °C thanks to the collective effect of C-(A)-S-H and ettringite (Rivera et al., 2016). It is worth mentioning that ettringite ($Ca_6Al_2(SO_4)_3(OH)_{12}\cdot 26H_2O$) is difficult to recognize by XRD method because it is not sensitive to trace phases, in contrast to the thermal analysis (Frost et al., 2003). The increase in the mass loss rate of the mixture was attributed to the promotion of the hydration products by SAP, regardless of with or without extra water. A second stage occurs at 400–600 °C, the calcium-rich C-A-S-H phase dehydrogenation and hydrotalcite dehydration are the main factors causing this phenomenon (Duan et al., 2017; Wongkeo et al., 2013). It is obvious from Fig. 12(a) and (b) that the total weight loss of pastes increases with the amount of SAP and additional water. Specifically, the mass loss within 250 °C increased progressively with adding SAP dosage, where the mixtures at each of the highest dosages (S0.3W0 and S0.2W25) increased by 16.46% and 18.66%, respectively, compared to the control group. It means a corresponding variation in the microstructure and reaction products of the AAS mortar. This happens because, the internal humidity of the matrix gradually declines with the hydration process, at this time SAP as an internal curing agent, under the negative pressure of capillary pores and the difference of internal and external humidity gradient begins to release water to maintain the humidity balance, while the water on the way of migration will react with the slag to promote the secondary hydration of the slag and thereby generating more hydration products

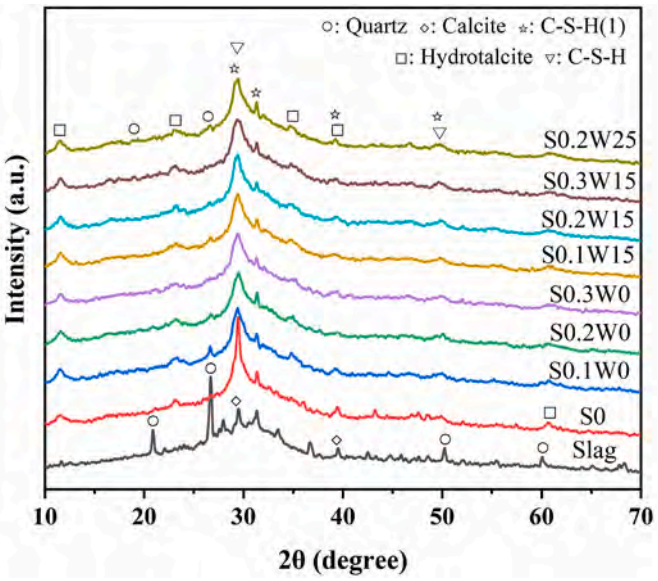

Fig. 13. XRD patterns of the AAS pastes.

like C-(A)-S-H gel phase (Yang et al., 2022b, 2022c). Although additional water works as well, it is not as directly effective as an internal curing agent. Between 400 and 600 temperatures, the mass loss of AAS mortar firstly decreases and then increases with the SAP content, as shown in Fig. 12(c) and (d). However, the addition of extra water resulted in an increase and then a decrease in mass loss over this temperature range (S0.2W0→S0.2W15→S0.2W25). This phenomenon suggests that whether it is SAP or extra water, their addition promotes the formation of gelling and favors the performance of the AAS mortar

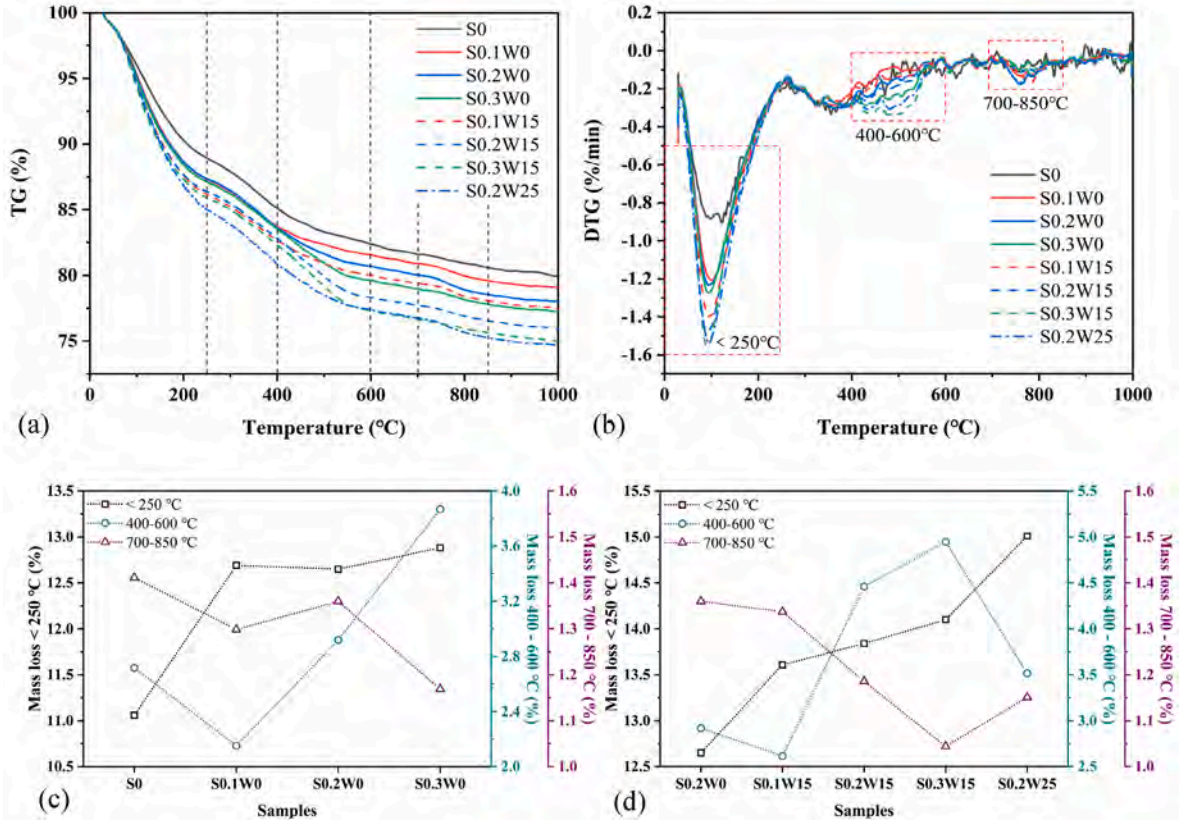

Fig. 12. TG-DTG curves and weight loss rate at different temperature regions of AAS pastes. (a) TG curves, (b) DTG curves, (c) weight loss rate at various SAP dosage, (d) weight loss rate at various extra water content.

(Powers and Brownyard, 2003). Nevertheless, it is necessary to ensure proper content. From the above, the following key findings emerge: (1) the introduction of SAP can actually promote the hydration reaction and increase the generation of extra hydration products, e.g., C-A-S-H gel phase; (2) the introduction of additional water supports the improvement of the hydration process. In a third step, Calcite ($CaCO_3$) is decarbonized at 700 °C–850 °C to form calcium oxide (CaO) and carbon dioxide (CO_2) (Long et al., 2021). As illustrated in Fig. 12(c) and (d), whether it was SAP or additional water, their introduction reduced the mass loss at this stage. Furthermore, with the SAP dosage and extra water content increase, the weight loss decreases, which suggests that the SAP and additional water facilitate the formation of C-A-S-H phases compared to the calcite phase ($CaCO_3$).

3.7. XRD analysis

The XRD patterns of AAS pastes at different SAP dosages and additional water content are shown in Fig. 13. A wide peak appears at about $2\theta = 29°–31°$, representing the small-range order of $CaO–Al_2O_3–MgO–SiO_2$ crystal structure in the slag (Richardson et al., 1994). The peak of quartz and calcite of the pastes are weakened compared to the raw material slag, as shown in Fig. 13. It appears that SAP strongly facilitates the rate of hydration and hydrotalcite formation. The C–S–H is foil-like when it is 100% slag (alkali-activated). Despite the added extra water resulting in a higher degree of hydration as well as the generation of more hydration products, free water is easily dissipated by evaporation when hardened in the natural environment. SAP, however, continuously releases the previously absorbed water to ensure the dynamic balance of humidity over time, and their presence is less affected by external factors. Furthermore, a new peak appears at $2\theta = 11.5°$ and 23.4° et., indicating that there are other hydration products such as Mg–Al hydrotalcite with interlamellar crystal. Because of the amorphous phase of calcium silicate hydrate (C–S–H), it presents a diffuse diffraction peak in the XRD pattern. A gel phase with insufficient crystallinity, as C–S–H (1), is also observed at 29.4°, 31.8° and 49.5° et., which is likely to occur in alkali-activated slag pastes (Zhang et al., 2015). With the increase of SAP content and water amount, the peak values of hydration products are slightly different. This is due to the introduction of SAP, which releases free water; the latter reacts with anhydrate slag, enhancing the hydration of the cementitious material and increasing the degree of hydration. In any case, the overall XRD pattern shows a very similar phase composition.

3.8. SEM analysis

Fig. 14 shows the SEM images of 28-days cured AAS mortars. Except for the pores introduced by SAP, there are very few large capillary pores. Overall, the SEM image of the S0.2W0 matrix is flatter and denser compared to the reference group. And the introduction of additional water will bring more pores to affect the development of strength. Especially when both SAP and water (e.g., S0.3W15) are in excess, it can cause a sharp decrease in compressive strength of AAS mortar due to the formation of larger pores, as shown in Fig. 14(d). The microcracks on the surface of the matrix might be due to the curing shrinkage of the sample (Puertas et al., 2004). SAP is subjected to volume reduction after the release of water, but it may not recover its original shape. At last, it becomes like a gel layer that covers the pore wall, leaving closed round pores or irregular pores with a diameter of about 50–200 μm, as clearly

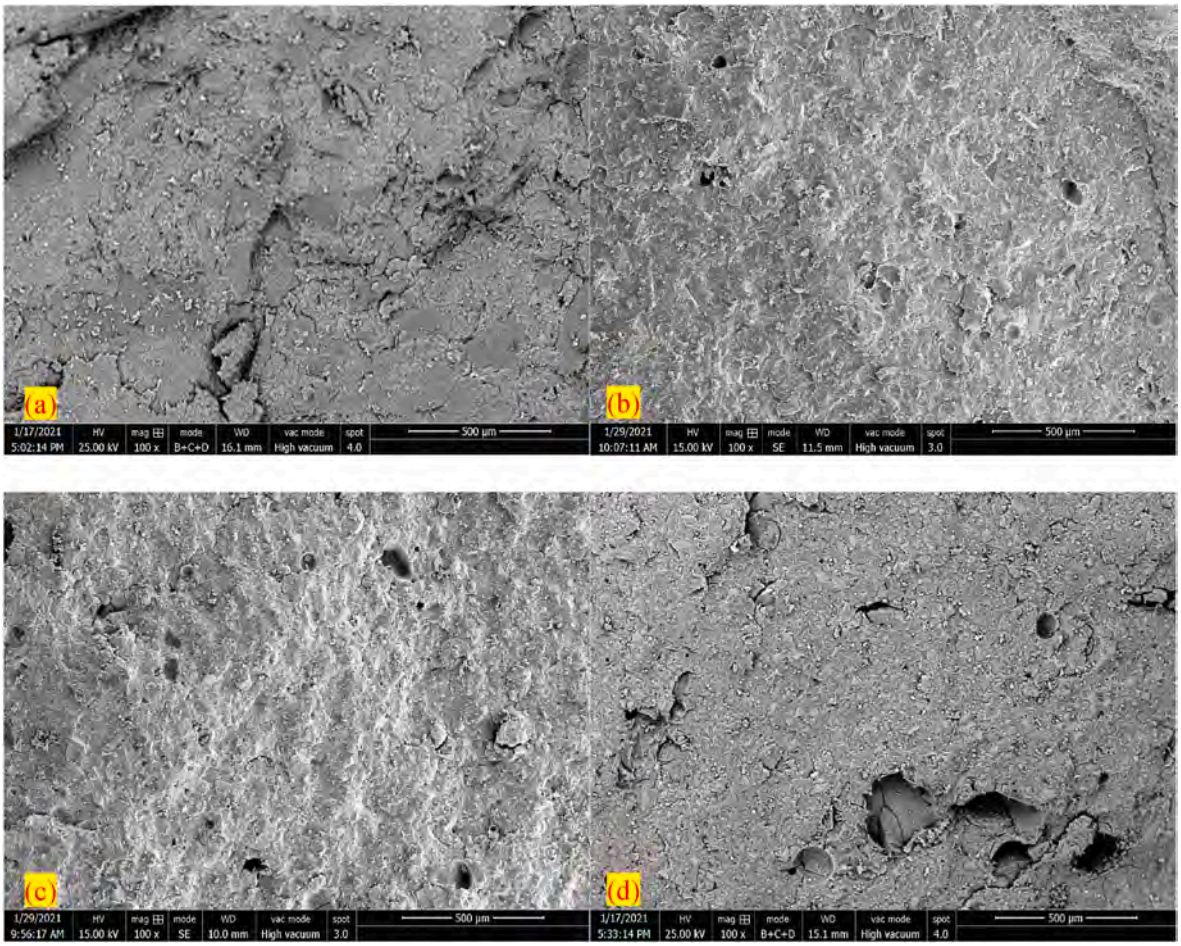

Fig. 14. The SEM images of AAS mortar. (a) S0, (b) S0.2W0, (c) S0.2W15, (d) S0.3W15.

shown in Fig. 14(b) ~ (d). Pore size is not only related to the particle size of SAP, but also to their ability to absorb water in different solutions. These harmful holes can impact the load bearing capacity of the structure.

3.9. Pore analysis

Fig. 15 shows the pore diameter and cumulative pore volume curves of AAS mortar after 28 days of curing at different SAP dosage and extra water content. It is not difficult to find that the introduction of SAP improves the percentage of gel pores in alkali slag mortar inside 0.01 μm. The greater the presence of these pores, the higher the degree of hydration. In addition, the presence of SAP, compared with reference samples, results in more micropores characterized by dimensions smaller than 0.1 μm and characterized by diameters between 0.1 and 1 μm. This further demonstrates that internal curing can result in a denser gel, which explains why the presence of SAP gives rise to increases in mortar strength (see Fig. 6). It is well known that porosity is one of the essential factors contributing to the differences in the properties (e.g., mechanical properties) of AAS mortars. The appropriate amount of SAP addition refines the pore distribution, because of more fine capillary pores or even gel pores, the structure of AAS mortar will get better densification and have stronger bearing capacity. However, as mentioned above, an excessive amount of SAP once the water is released results in the presence of macro voids. Since SAP expands tens or hundreds of times in volume after absorbing water, compressing the surrounding pastes, their volume contraction after subsequent water release leaves large foot-diameter holes in the matrix (see Fig. 14). The presence of these voids drops the performance of the AAS mortar. In fact, after 10 μm, the curves related to the specimens with the largest amounts of SAP begin to rise gradually. This indicates that the SAP, in these cases, leads to the occurrence of a greater presence of macropores, like the ones identified in Fig. 13. Therefore, when the negative effect of introducing macropores is greater than the positive effect of promoting hydration, it will be directly reflected in the decrease of strength.

According to MIP data, the addition of SAP reduces the total porosity of alkali activated mortar products and changes the pore structure. The hydration process is improved and the pores of AAS are reduced by the filling action of hydration products and the nucleation effect of SAP particles. This is the cause of the increase in strength that occurs after adding an appropriate dose of SAP.

As expected, the overall porosity of each group increased significantly with increasing water, especially in the case of additional water with a mass ratio of 15 times and 0.3% SAP content. Although the introduction of water can promote the hydration of slag, when SAP is excessive, the number of internal macropores increases. In addition, excessive water release and free water increase the total porosity, resulting in many interconnected pores. Hence, when water enters the specimen under pressure, the presence of these interconnected macropores accelerates the passage of free water (Haha et al., 2011), thus reducing the impermeability of AAS mortar, as experimentally found in this study.

Collins (Collins and Sanjayan, 1999) concluded that the shrinkage pore size is mainly distributed between 0.002 μm and 0.05 μm. Although the addition of SAP increases the number of small pores and gels, resulting in an increase in total porosity, the release of water by the SAP

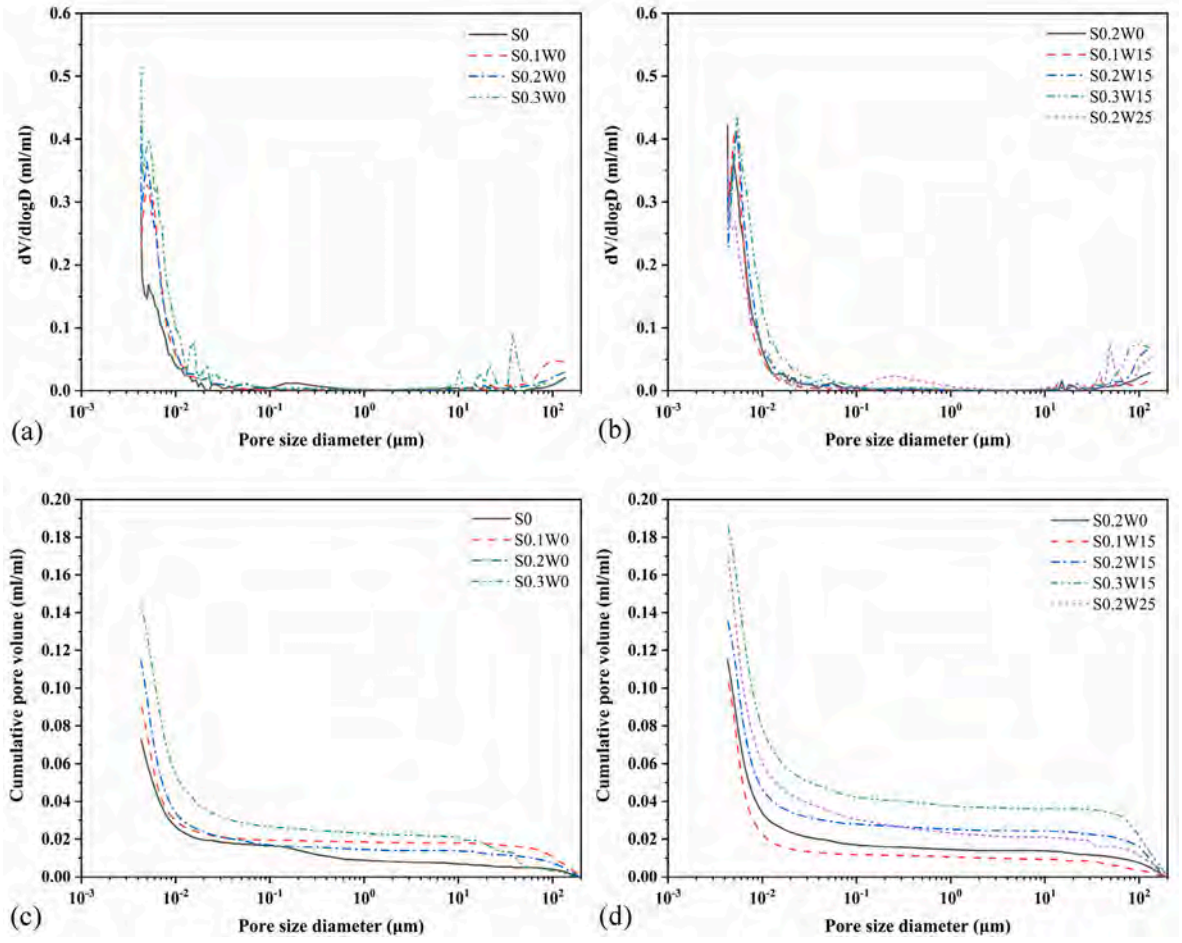

Fig. 15. MIP results of all mixtures at 28 days. (a) and (c): pore size diameter at various SAP dosage, (b) and (d): cumulative pore volume at different additional water content.

allows it to balance the loss of water due to hydration processes and external drying; in addition, this change in microstructure, as seen, gives rise to a significant increase in resistance to freeze-thaw cycles and also gives beneficial effects in terms of reducing autogenous shrinkage (Fig. 6).

4. Conclusions

This study highlighted the feasibility and beneficial effects of using SAP as an internal curing agent in the production of alkali slag mortar. The effects of SAP dosage and additional water content on setting time, strength, shrinkage, frost resistance, and impermeability of AAS were studied. The following conclusions are obtained based on this study:

1. SAP showed a strong liquid absorption ability at pH = 7. However, the presence of multi-ions in alkali solution such as Ca^{2+}, Al^{3+} with the increase of the pH value of the solution enhanced the cross-linking of SAP molecular chains, destroyed the electronic barrier effect, and reduced the liquid absorption ability of SAP.
2. Compared with S0, the setting times and the time of the peak hydration heat of AAS mortar increased progressively with increasing SAP dosage and additional water content. In addition, due to the improved degree of hydration, the cumulative heat release in the cases of the higher dosages of SAP and additional water contents was higher than that of reference sample.
3. The addition of SAP improved the impermeability and frost resistance of AAS mortar; its use is therefore particularly suitable in harsh climates for improving frost resistance, due to its effect of reducing hydrostatic pressure within the system matrix. However, the addition of an excessive amount of additional water caused the porosity and number of pores with larger diameters to increase, resulting in a reduction in the durability of the material.
4. An appropriate amount of SAP and water can improve the compressive strength of the AAS mortar. In fact, increases in compressive strength of about 15.6% over the reference samples at 28 days were recorded in the best cases. However, an excessive amount of SAP and water resulted in the opposite effect, with the presence of many macropores in the size range of 50–100 μm in the material, and consequent reduction in strength.
5. The autogenous shrinkage of AAS pastes was significantly reduced by the internal curing of SAP. Although the reduction effect was greater the higher the SAP dosage and water content, the autogenous shrinkage of AAS could not be completely eliminated.

CRediT authorship contribution statement

Peng Shi: Writing – review & editing, Writing – original draft, Methodology, Investigation, Conceptualization, Data curation, Formal analysis, Visualization. **Devid Falliano:** Writing – review & editing, Validation, Methodology, Conceptualization, Writing – original draft. **Federico Vecchio:** Writing – review & editing, Validation. **Giuseppe Carlo Marano:** Writing – review & editing, Supervision, Methodology, Conceptualization.

Declaration of competing interest

The authors declare that they have no known competing financial interests or personal relationships that could have appeared to influence the work reported in this paper.

Data availability

Data will be made available on request.

Acknowledgements

This work was financially supported by China Scholarship Council (No. 202106650016). The support from Politecnico di Torino is gratefully acknowledged.

References

Adediran, A., Yliniemi, J., Moukannaa, S., et al., 2023. Enhancing the thermal stability of alkali-activated Fe-rich fayalite slag-based mortars by incorporating ladle and blast furnace slags: physical, mechanical and structural changes. Cement Concr. Res. 166, 107098 https://doi.org/10.1016/j.cemconres.2023.107098.

Almeida, F.C.R., Klemm, A.J., 2018. Efficiency of internal curing by superabsorbent polymers (SAP) in PC-GGBS mortars. Cement Concr. Compos. 88, 41–51. https://doi.org/10.1016/j.cemconcomp.2018.01.002.

ASTM, 2014. C1698-19: Standard Test Method for Autogenous Strain of Cement Paste and Mortar. ASTM International, West Conshohocken, PA, USA. https://doi.org/10.1520/C1698-19.

ASTM, 2018. C349-18: Standard Test Method for Compressive Strength of Hydraulic Cement Mortars (Using Portions of Prisms Broken in Flexure). ASTM International, West Conshohocken, PA, USA. https://doi.org/10.1520/C0349-18.

Bayati, M., Adelzade Saadabadi, L., Sedaghatdoost, A., 2023. Performance of self-healed alkali-activated slag mortar at elevated temperature. J. Mater. Civ. Eng. 35 (7), 04023178 https://doi.org/10.1061/JMCEE7.MTENG-13977.

Boshoff, W., Mechtcherine, V., Snoeck, D., et al., 2020. The effect of superabsorbent polymers on the mitigation of plastic shrinkage cracking of conventional concrete, results of an inter-laboratory test by RILEM TC 260-RSC. Mater. Struct. 53 (79), 1–16. https://doi.org/10.1617/s11527-020-01516-6.

Chen, P., Wang, J., Wang, L., et al., 2019. Perforated cenospheres: a reactive internal curing agent for alkali activated slag mortars. Cement Concr. Compos. 104, 103351 https://doi.org/10.1016/j.cemconcomp.2019.103351.

Chen, W., Li, B., Guo, M.Z., et al., 2023. Impact of heat curing regime on the compressive strength and drying shrinkage of alkali-activated slag mortar. Developments in the Built Environment 14, 100123. https://doi.org/10.1016/j.dibe.2023.100123.

Collins, F., Sanjayan, J.G., 1999. Strength and shrinkage properties of alkali-activated slag concrete containing porous coarse aggregate. Cement Concr. Res. 29 (4), 607–610. https://doi.org/10.1016/S0008-8846(98)00203-8.

Collins, F., Sanjayan, J.G., 2000. Effect of pore size distribution on drying shrinking of alkali-activated slag concrete. Cement Concr. Res. 30 (9), 1401–1406. https://doi.org/10.1016/S0008-8846(00)00327-6.

Cusson, D., Hoogeveen, T., 2008. Internal curing of high-performance concrete with pre-soaked fine lightweight aggregate for prevention of autogenous shrinkage cracking. Cement Concr. Res. 38 (6), 757–765. https://doi.org/10.1016/j.cemconres.2008.02.001.

Duan, P., Yan, C., Zhou, W., 2017. Compressive strength and microstructure of fly ash based geopolymer blended with silica fume under thermal cycle. Cement Concr. Compos. 78, 108–119. https://doi.org/10.1016/j.cemconcomp.2017.01.009.

Duxson, P., Lukey, G.C., van Deventer JSJ, 2007. Physical evolution of Na-geopolymer derived from metakaolin up to 1000 °C. J. Mater. Sci. 42, 3044–3054. https://doi.org/10.1007/s10853-006-0535-4.

Esteves, L.P., Cachim, P., Ferreira, V.M., 2007. Mechanical Properties of Cement Mortars with Superabsorbent Polymers. In Advances in Construction Materials (Grosse CU. Springer, Berlin, Heidelberg, pp. 451–462. https://doi.org/10.1007/978-3-540-72448-3_45.

Fang, G., Bahrami, H., Zhang, M., 2018. Mechanisms of autogenous shrinkage of alkali-activated fly ash-slag pastes cured at ambient temperature within 24 h. Construct. Build. Mater. 171, 377–387. https://doi.org/10.1016/j.conbuildmat.2018.03.155.2019.

Filho, J.R.T., Vermoesen, E., Mannekens, E., et al., 2021. Enhanced durability performance of cracked and uncracked concrete by means of smart in-house developed superabsorbent polymers with alkali-stable and -unstable crosslinkers. Construct. Build. Mater. 297, 123812 https://doi.org/10.1016/j.conbuildmat.2021.123812.

Frost, R.L., Martens, W., Ding, Z., et al., 2003. DSC and high-resolution TG of synthesized hydrotalcites of Mg and Zn. J. Therm. Anal. Calorim. 71 (2), 429–438. https://doi.org/10.1023/A:1022835305846.

Fu, C., Ye, H., Lei, A., et al., 2020. Effect of novel superabsorbent polymer composites on the fresh and hardened properties of alkali-activated slag. Construct. Build. Mater. 232, 117225 https://doi.org/10.1016/j.conbuildmat.2019.117225.

GB/T, 2009. 50082-2009 Standard for Test Methods of Long-Term Performance and Durability of Ordinary Concrete. Beijing: China Construction Industry Press, China.

Haha, M., Lothenbach, B., Saout, G., et al., 2011. Influence of slag chemistry on the hydration of alkali-activated blast-furnace slag - Part I: effect of MgO. Cement Concr. Res. 41 (9), 955–963. https://doi.org/10.1016/j.cemconres.2011.05.002.

Huang, D., Chen, P., Peng, H., et al., 2022. Drying shrinkage performance of medium-Ca alkali-activated fly ash and slag pastes. Cement Concr. Compos. 130, 104536 https://doi.org/10.1016/j.cemconcomp.2022.104536.

Jensen, O.M., Hansen, P.F., 2001. Autogenous deformation and RH-change in perspective. Cement Concr. Res. 31 (12), 1859–1865. https://doi.org/10.1016/S0008-8846(01)00501-4.

JGJ/T, 2009. 70-2009: Standard for Test Method of Basic Properties of Construction Mortar. Beijing: China Construction Industry Press, China.

Kalina, L., Bílek, V., Bartoníčková, E., et al., 2020. Doubts over capillary pressure theory in context with drying and autogenous shrinkage of alkali-activated materials.

Construct. Build. Mater. 248, 118620 https://doi.org/10.1016/j.conbuildmat.2020.118620.
Kumarappa, B.D., Peethamparan S, S., Ngami, M., 2018. Autogenous shrinkage of alkali activated slag mortars: basic mechanisms and mitigation methods. Cement Concr. Res. 109, 1–9. https://doi.org/10.1016/j.cemconres.2018.04.004.
Lee, H.X.D., Wong, H.S., Buenfeld, N.R., 2010. Potential of superabsorbent polymer for self-sealing cracks in concrete. Adv. Appl. Ceram. 109 (5), 296–302. https://doi.org/10.1179/174367609X459559.
Lee, N.K., Abate, S.Y., Kim, H.K., 2018. Use of recycled aggregates as internal curing agent for alkali-activated slag system. Construct. Build. Mater. 159, 286–296. https://doi.org/10.1016/j.conbuildmat.2017.10.110.
Liu, J., Ou, Z., Mo, J., et al., 2017. The effect of SCMs and SAP on the autogenous shrinkage and hydration process of RPC. Construct. Build. Mater. 155, 239–249. https://doi.org/10.1016/j.conbuildmat.2017.08.061.
Long, W.J., Xie, J., Zhang, X., et al., 2021. Hydration and microstructure of calcined hydrotalcite activated high-volume fly ash cementitious composite. Cement Concr. Compos. 123, 104213 https://doi.org/10.1016/j.cemconcomp.2021.104213.
Ma, H., Zhu, H., Wu, C., et al., 2020. Effect of shrinkage reducing admixture on drying shrinkage and durability of alkali-activated coal gangue-slag material. Construct. Build. Mater. 270, 121372 https://doi.org/10.1016/j.conbuildmat.2020.121372.
Mavroulidou, M., Shah, S., 2021. Alkali-activated slag concrete with paper industry waste. Waste Manag. Res. 39 (3), 466–472. https://doi.org/10.1177/0734242X20983890.
Mechtcherine, V., Gorges, M., Schroefl, C., et al., 2014. Effect of internal curing by using superabsorbent polymers (SAP) on autogenous shrinkage and other properties of a high-performance fine-grained concrete: results of a RILEM round-robin test. Mater. Struct. 47, 541–562. https://doi.org/10.1617/s11527-013-0078-5.
Mechtcherine, V., Schröfl, C., Reichardt, M., et al., 2019. Recommendations of RILEM TC 260-RSC for using superabsorbent polymers (SAP) for improving freeze–thaw resistance of cement-based materials. Mater. Struct. 52 (75), 1–7. https://doi.org/10.1617/s11527-019-1375-4.
Mechtcherine, V., Wyrzykowski, M., Schröfl, C., et al., 2021. Application of super absorbent polymers (SAP) in concrete construction—update of RILEM state-of-the-art report. Mater. Struct. 54 (80), 1–20. https://doi.org/10.1617/s11527-021-01668-z.
Mo, J., Ou, Z., Zhao, X., et al., 2017. Influence of superabsorbent polymer on shrinkage properties of reactive powder concrete blended with granulated blast furnace slag. Construct. Build. Mater. 146, 283–296. https://doi.org/10.1016/j.conbuildmat.2017.04.105.
Neto, A.A.M., Cincotto, M.A., Repette, W., 2008. Drying and autogenous shrinkage of pastes and mortars with activated slag cement. Cement Concr. Res. 38 (4), 565–574. https://doi.org/10.1016/j.cemconres.2007.11.002.
Oh, S., Choi, Y.C., 2018. Superabsorbent polymers as internal curing agents in alkali activated slag mortars. Construct. Build. Mater. 159 (Jan.20), 1–8. https://doi.org/10.1016/j.conbuildmat.2017.10.121.
Pacheco-Torgal, F., Abdollahnejad, Z., Camões, A.F., et al., 2012. Durability of alkali-activated binders: a clear advantage over Portland cement or an unproven issue? Construct. Build. Mater. 30, 400–405. https://doi.org/10.1016/j.conbuildmat.2011.12.017.
Philleo, R., 1991. Concrete science and reality. In: Materials Science of Concrete II (Skalny JP and Mindess S. American Ceramic Society, Westerville, OH, pp. 1–8.
Powers, T.C., Brownyard, T.L., 2003. Studies of the physical properties of hardened Portland cement paste part 9. general summary of findings on the properties of hardened Portland cement paste. Concr. Int. 25 (9), 31–42. https://doi.org/10.1016/10.14359/15301.
Provis, J.L., 2014. Geopolymers and other alkali activated materials: why, how, and what? Mater. Struct. 47 (1–2), 11–25. https://doi.org/10.1617/s11527-013-0211-5.
Puertas, F., Jiménez, A.F., Varela, M.T.B., 2004. Pore solution in alkali-activated slag cement pastes, Relation to the composition and structure of calcium silicate hydrate. Cement Concr. Res. 34, 139–148. https://doi.org/10.1016/S0008-8846(03)00254-0.
Richardson, I.G., Brough, A.R., Groves, G.W., et al., 1994. The characterization of hardened alkali-activated blast-furnace slag pastes and the nature of the calcium silicate hydrate (C-S-H) phase. Cement Concr. Res. 24 (5), 813–829. https://doi.org/10.1016/0008-8846(94)90002-7.
Rivera, O.G., Long, W.R., Weiss Jr., C.A., et al., 2016. Effect of elevated temperature on alkali-activated geopolymeric binders compared to Portland cement-based binders. Cement Concr. Res. 90, 43–51. https://doi.org/10.1016/j.cemconres.2016.09.013.
Sakulich, A.R., Bentz, D.P., 2013. Mitigation of autogenous shrinkage in alkali activated slag mortars by internal curing. Mater. Struct. 46 (8), 1355–1367. https://doi.org/10.1617/s11527-012-9978-z.
Schröfl, C., Mechtcherine, V., Gorges, M., 2012. Relation between the molecular structure and the efficiency of superabsorbent polymers (SAP) as concrete admixture to mitigate autogenous shrinkage. Cement Concr. Res. 42 (6), 865–873. https://doi.org/10.1016/j.cemconres.2012.03.011.
Shen, D., Shi, H., Tang, X., et al., 2016. Effect of internal curing with super absorbent polymers on residual stress development and stress relaxation in restrained concrete ring specimens. Construct. Build. Mater. 120 (Sep.1), 309–320. https://doi.org/10.1016/j.conbuildmat.2016.05.048.
Snoeck, D., Jensen, O.M., Belie, N.D., 2015. The influence of superabsorbent polymers on the autogenous shrinkage properties of cement pastes with supplementary cementitious materials. Cement Concr. Res. 74, 59–67. https://doi.org/10.1016/j.cemconres.2015.03.020.
Snoeck, D., Dewanckele, J., Cnudde, V., et al., 2016. X-ray computed microtomography to study autogenous healing of cementitious materials promoted by superabsorbent polymers. Cement Concr. Compos. 65, 83–93. https://doi.org/10.1016/j.cemconcomp.2015.10.016.
Song, C., Choi, Y.C., Choi, S., 2016. Effect of internal curing by superabsorbent polymers - internal relative humidity and autogenous shrinkage of alkali-activated slag mortars. Construct. Build. Mater. 123, 198–206. https://doi.org/10.1016/j.conbuildmat.2016.07.007.
Sun, B., Wu, H., Song, W., et al., 2020. Hydration, microstructure and autogenous shrinkage behaviors of cement mortars by addition of superabsorbent polymers. Front. Struct. Civ. Eng. 14, 1274–1284. https://doi.org/10.1007/s11709-020-0656-x.
Tenório Filho, J.R., De Belie, N., Snoeck, D., 2023. Reaching beyond internal curing: the effects of superabsorbent polymers on the durability of reinforced concrete structures. In: Jędrzejewska, A., Kanavaris, F., Azenha, M., Benboudjema, F., Schlicke, D. (Eds.), International RILEM Conference on Synergising Expertise towards Sustainability and Robustness of Cement-Based Materials and Concrete Structures. SynerCrete 2023, RILEM Bookseries, vol. 44. Springer, Cham, pp. 933–941. https://doi.org/10.1007/978-3-031-33187-9_85.
Trincal, V., Multon, S., Benavent, V., et al., 2022. Shrinkage mitigation of metakaolin-based geopolymer activated by sodium silicate solution. Cement Concr. Res. 162, 106993 https://doi.org/10.1016/j.cemconres.2022.106993.
Tu, W., Zhu, Y., Fang, G., et al., 2018. Internal curing of alkali-activated fly ash-slag pastes using superabsorbent polymer. Cement Concr. Res. 116, 179–190. https://doi.org/10.1016/j.cemconres.2018.11.018.
Turner, L.K., Collins, F.G., 2013. Carbon dioxide equivalent (CO_2-e) emissions: a comparison between geopolymer and OPC cement concrete. Construct. Build. Mater. 43, 125–130. https://doi.org/10.1016/j.conbuildmat.2013.01.023.
Vafaei, B., Farzanian, K., Ghahremaninezhad, A., 2019. The influence of superabsorbent polymer on the properties of alkali-activated slag pastes. Construct. Build. Mater. 236, 117525 https://doi.org/10.1016/j.conbuildmat.2019.117525.
van Deventer JSJ, Provis, J.L., Duxson, P., 2012. Technical and commercial progress in the adoption of geopolymer cement. Miner. Eng. 29, 89–104. https://doi.org/10.1016/j.mineng.2011.09.009.
Wang, S., Pu, X., Scrivener, K.L., et al., 1995. Alkali-activated slag cement and concrete: a review of properties and problems. Adv. Cement Res. 7 (27), 93–102. https://doi.org/10.1680/adcr.1995.7.27.93.
Winnefeld, F., Gluth, G.J.G., Bernal, S.A., et al., 2020. RILEM TC 247-DTA round robin test: sulfate resistance, alkali-silica reaction and freeze-thaw resistance of alkali-activated concretes. Mater. Struct. 53 (140), 1–17. https://doi.org/10.1617/s11527-020-01562-0.
Wongkeo, W., Thongsanitgarn, P., Chindaprasirt, P., et al., 2013. Thermogravimetry of ternary cement blends: effect of different curing methods. J. Therm. Anal. Calorim. 113, 1079–1090. https://doi.org/10.1007/s10973-013-3017-3.
Yang, J., Snoeck, D., Belie, N.D., et al., 2021. Effect of superabsorbent polymers and expansive additives on the shrinkage of alkali-activated slag. Cement Concr. Compos. 123, 104218 https://doi.org/10.1016/j.cemconcomp.2021.104218.
Yang, J., Sun, Z., Belie, N.D., et al., 2022a. Mitigating plastic shrinkage cracking in alkali-activated slag systems by internal curing with superabsorbent polymers. Cement Concr. Compos. 134, 104784 https://doi.org/10.1016/j.cemconcomp.2022.104784.
Yang, Z., Shi, P., Zhang, Y., et al., 2022b. Influence of liquid-binder ratio on the performance of alkali-activated slag mortar with superabsorbent polymer. J. Build. Eng. 48, 103934 https://doi.org/10.1016/j.jobe.2021.103934.
Yang, Z., Shi, P., Zhang, Y., et al., 2022c. Effect of superabsorbent polymer introduction on properties of alkali-activated slag mortar. Construct. Build. Mater. 340, 127541 https://doi.org/10.1016/j.conbuildmat.2022.127541.
Yang, J., Sun, Z., De Belie, N., et al., 2023. Self-healing ability of cracks in alkali-activated slag systems incorporating superabsorbent polymers. Cement Concr. Res. 170, 107183 https://doi.org/10.1016/j.cemconres.2023.107183.
Ye, H., Radlińska, A., 2017. Shrinkage mitigation strategies in alkali-activated slag. Cement Concr. Res. 101, 131–143. https://doi.org/10.1016/j.cemconres.2017.08.025.
Ye, H., Cartwright, C., Rajabipour, F., et al., 2017. Understanding the drying shrinkage performance of alkali-activated slag mortars. Cement Concr. Compos. 76, 13–24. https://doi.org/10.1016/j.cemconcomp.2016.11.010.
Yuan, B., Yu, Q.L., Dainese, E., et al., 2017. Autogenous and drying shrinkage of sodium carbonate activated slag altered by limestone powder incorporation. Construct. Build. Mater. 153, 459–468. https://doi.org/10.1016/j.conbuildmat.2017.07.112.
Zhang, Z.H., Provis, J.L., Reid, A., et al., 2015. Mechanical, thermal insulation, thermal resistance and acoustic absorption properties of geopolymer foam concrete. Cement Concr. Compos. 62, 97–105. https://doi.org/10.1016/j.cemconcomp.2015.03.013.
Zhang, B., Zhu, H., Cheng, Y., et al., 2022. Shrinkage mechanisms and shrinkage-mitigating strategies of alkali-activated slag composites: a critical review. Construct. Build. Mater. 318, 125993 https://doi.org/10.1016/j.conbuildmat.2021.125993.
Zhao, H., Jiang, K., Di, Y., et al., 2019. Effects of curing temperature and superabsorbent polymers on hydration of early-age cement paste containing a CaO-based expansive additive. Mater. Struct. 52 (6) https://doi.org/10.1617/s11527-019-1407-0, 108.1-108.11.
Zhong, P., Wyrzykowski, M., Toropovs, N., et al., 2019. Internal curing with superabsorbent polymers of different chemical structures. Cement Concr. Res. 123, 105789 https://doi.org/10.1016/j.cemconres.2019.105789.